THE ASTROPHYSICAL JOURNAL, 460:449–459, 1996 March 20
© 1996. The American Astronomical Society. All rights reserved. Printed in U.S.A.

A SEARCH FOR PULSATIONS IN FOUR LATE-TYPE GIANTS[1]

SCOTT HORNER[2,3]
Department of Astronomy and Astrophysics, The University of Chicago, 5640 S. Ellis Avenue, Chicago, IL 60637; and High Altitude Observatory, National Center for Atmospheric Research,[4] P.O. Box 3000, Boulder, CO 80307-3000
Received 1994 September 1; accepted 1995 September 25

ABSTRACT

I observed four late-type giant stars to search for oscillations similar to those observed on Arcturus. For these observations, I used the Kitt Peak National Observatory Coudé Feed telescope and Fiber Optic Echelle spectrograph. I observed α Ari, γ Per, ε Tau, and α Aur (a close binary composed of two G giants) for 12 nights, observing each star ~5 times per night in order to detect oscillations with periods on the order of 2 days. I chose these stars, which range in spectral types from G8 III to K2 III, because of their spectral similarity to Arcturus (α Boo, K1 III), for which earlier observations revealed oscillations.

No oscillations were detected on any of the four stars observed in this campaign. The upper limits of the oscillation amplitudes at periods comparable to those seen on Arcturus fall well below those observed for Arcturus. Continued observations of Arcturus are required to determine whether the observed period and amplitude are stable, or if the structure of Arcturus is different from the late-type giants observed in this campaign.

Subject headings: stars: late-type — stars: oscillations — techniques: radial velocities

1. INTRODUCTION

Asteroseismic observations of stars other than the Sun require sophisticated instrumentation, observation, and data reduction techniques that are still under development (for a review of asteroseismology, see Brown & Gilliland 1994). There are two methods for detecting global stellar oscillations: one method is to measure the changes in the integrated intensity of the star resulting from the oscillation using very precise relative photometry (see Gilliland & Brown 1988; Kjeldsen & Frandsen 1992; Gilliland et al. 1991; Gilliland et al. 1993), and the other technique is to detect the motion of the stellar photosphere by measuring the Doppler shift of spectral lines formed there. The Doppler method consists of two different approaches, the non-multiplex approach and the multiplex approach. The non-multiplex approach utilizes a few very narrow bandpasses, using either narrow filters or a Fabry-Perot interferometer, to monitor the wings of one or a few spectral lines. The changes in relative intensity between the narrow bandpasses on the blue and red wings of a spectral line then allow determination of the shift of that line to high precision (see Pottasch, Butcher, & van Hoesel 1992). The multiplex approach utilizes a traditional echelle spectrograph to sample the shifts of a large number of spectral lines. The Doppler shift of a single line cannot be determined to high precision, but using the large number of lines observable with an echelle allows for very precise overall measurements (Brown 1990; Brown et al. 1991).

Because of the wealth of knowledge obtained from helioseismology and our vested interest, as residents of Earth, in Sun-like stars, there is a strong impetus to observe oscillations of these stars. Solar oscillations have a period of ≈5 minutes, with a peak amplitude of 3 μmag in integrated intensity and a peak velocity of 15 cm s^{-1} per individual mode, values that make a truly Sun-like star inaccessible with standard instrumentation. So far there have been only tentative observations of Sun-like nonradial oscillations of any star other than the Sun. The best evidence to date is presented by Pottasch et al. (1992) observing α Cen A using a Fabry-Perot velocity analyzer (the non-multiplex technique). While the non-multiplex method may suffice for observations of α Cen A, observations of fainter stars will require different instrumentation.

Late-type giant stars are believed to have larger oscillation amplitudes in both broadband intensity and velocity (Christensen-Dalsgaard & Frandsen 1983). Indeed, observations of Arcturus (α Boo, K1 III) revealed oscillations with a period of 1.84 days and an amplitude of 160 m s^{-1} that may be the result of Sun-like *p*-mode oscillations (Smith, McMillan, & Merline 1987; Cochran 1988, Belmonte et al. 1990). Because of their large amplitude, which allow for easier detection, and their long periods, which allow for longer exposure times (which in turn allow the use of a smaller telescope), late-type giants like Arcturus serve as a good test of the instrumentation, observation, and data analysis techniques used for this study. There are also a large number of giants bright enough to produce the required precision within the constraints of the exposure times.

The target stars and the basic instrumention used for these observations are described in § 2. The details of the instrumentation used and the observation procedures are described in § 3. The data reduction and analysis procedures used to determine the Doppler shifts from the echelle images are discussed briefly in § 4. In § 5, the results of the analyses are presented, and § 6 contains concluding comments. The derivation of the least-squares shift tech-

[1] Presented as a dissertation to the Department of Astronomy and Astrophysics, University of Chicago, in partial fulfillment of the requirements for the Ph.D. degree.

[2] Visiting Astronomer, Kitt Peak National Observatory, National Optical Astronomy Observatories, operated by AURA, Inc., under contract with the National Science Foundation.

[3] Now at Astronomy and Astrophysics, Pennsylvania State University, 525 Davey Laboratory, University Park, PA 16802-6305.

[4] The National Center for Atmospheric Research is sponsored by the National Science Foundation.

© American Astronomical Society • Provided by the NASA Astrophysics Data System

nique for blended or superimposed spectra is presented in the Appendix.

2. TARGET STARS

I observed four late-type giant stars, α Ari, γ Per, ϵ Tau, and α Aur, using the Kitt Peak National Observatory (KPNO) Coudé Feed telescope (0.9 m), Fiber Optic Echelle spectrograph (FOE) (see Ramsey & Huenemoerder 1986), and TI3 detector (800 × 800, 15 μm pixels). The observations were made over a 12 day period from 1991 October 30 to 1991 November 10. I obtained multiple exposures of α Ari, α Aur, and γ Per five times a night on 10.5 of these nights. Since ϵ Tau required long exposure times, it was typically observed three times a night. A 200 μm optical fiber connects the Coudé Feed to the FOE. The region of the spectrum observed ranged from 480 to 600 nm. The signal-to-noise ratio per resolution element in the dispersion direction is $\approx$200 at the blaze function peak, which was centered on the detector, and $\approx$140 at edges of the detector. The resolution of the spectrograph in the configuration used was 41,000 at 515 nm. Each echelle order is $\approx$4.5 nm wide, with a velocity of 100 m s^{-1} corresponding to a shift of 0.0276 pixels.

Table 1 lists the stars observed, their positions, spectral types, V-band magnitudes, exposure times, and rough estimates of their fundamental periods. The estimate of the fundamental period was used to further select the target stars from the list of candidate target stars for similarity to Arcturus; it is not known whether the Arcturus pulsations are radial ($l = 0$) or nonradial ($l > 0$), though Hatzes & Cochran (1994) argue from the period of the oscillations they observed in 1992 that they are radial. To estimate the fundamental periods, I calculated the luminosities of these stars using the parallax and apparent visual magnitudes listed in the Bright Star Catalogue (Hoffleit & Jaschek 1982), and the bolometric correction from Table 3.5 of Mihalas & Binney (1981). Then I calculated the radii of these stars using the calculated luminosities and the effective temperatures listed in Table 3.5 of Mihalas & Binney. For stars other than α Aur, I used the main-sequence mass-luminosity relation to estimate the upper limits to the masses of the stars. Using these estimates of the stellar radii and masses, I calculated rough estimates of the fundamental periods for these stars. The main-sequence mass-luminosity relation overestimates the mass of giants, so the calculated period should be less than the true fundamental period, but not by much since $P \propto M^{-1/2}$. For α Aur, I obtained the masses of the two components from Batten, Hill, & Lu (1991). Comparing these masses to the masses estimated from the main-sequence mass-luminosity relation, the fundamental periods estimated using this method are underestimates by approximately a factor of 2. For comparison, the estimated fundamental period of Arcturus calculated in this manner is 2.0 days.

I observed the four stars for oscillations with periods on the order of 2 days. I selected these stars because of their spectral similarity to Arcturus, their brightness, and their fundamental periods of $\sim$1 day. They range in spectral types from G8 III to K2 III. One of these stars (ϵ Tau) is a member of the Hyades and thus is of special interest. The Capella system (α Aur) is also of special interest because it is a close binary system composed of two G giants with known masses and angular diameters. The spectroscopic primary is the cooler, dimmer one of the pair (Bagnuolo & Sowell 1988). The spectroscopic secondary is rapidly rotating compared to the spectroscopic primary (50 km s^{-1} and 7 km s^{-1}, respectively; Fekel, Moffett, & Henry 1986), and hotter, so it has fewer, broader lines compared to the primary (see Figs. 1 and 2 of Pilachowski & Sowell 1992). Walker et al. (1989) observed α Ari and concluded that there were no velocity variations of amplitude of 30 m s^{-1} or more on timescales of less than a month.

3. OBSERVATIONS

I installed a molecular iodine (I_2) absorption cell (see Cochran & Hatzes 1990; Marcy & Butler 1992) in the optical path between the Coudé Feed telescope and the entrance optics of the optical fiber. The spectral lines of the I_2 gas are then superimposed over the stellar spectrum, establishing a wavelength reference. Sets of exposures where taken of the target stellar spectra with the I_2 spectrum superimposed three to five times per night of the run.

Each night, I obtained several exposures of each of the program stars without the I_2 cell in the beam for use as reference spectra. Also, at the beginning and end of each night, I observed γ Cas and β Ori with the I_2 cell in the beam. Both γ Cas and β Ori are rapidly rotating B stars with relatively featureless spectra; thus, these observations are approximations of the I_2 absorption spectrum without stellar spectral lines. I also obtained exposures of the I_2 spectrum using the flat-field quartz lamp at the beginning and end of each night. All these exposures are used as references to determine the relative shift of the I_2 and stellar spectra in the observations where the I_2 and stellar spectra are superimposed (see § 4.3).

A second 200 μm optical fiber connects the FOE to a hollow-cathode reference lamp which provides a secondary wavelength calibration source. I used a thorium-argon (ThAr) hollow-cathode lamp because of its line structures in the blue. Therefore, each exposure has 10 echelle orders of stellar spectrum, with or without the I_2 cell absorption superimposed, interleaved with 10 echelle orders of ThAr emission spectrum. To diffuse the light from the ThAr lamp cathode, I used a frosted glass plate. I used neutral density filters to maintain consistent exposure levels from the lamp for the different exposure times of the various stars. Normally, a double-fiber scrambler (see Ramsey 1988; Ramsey et al. 1991) should be used with observations calibrated

TABLE 1

PARAMETERS OF OBSERVED STARS

Star	R.A.	Dec.	Spectral Type	V	t(minutes)	P(days)
α Ari	2^h7^m	23°27′	K2 III	2.00	8	>1.8
γ Per	3 5	53 30	G8 III	2.93	19	>2.6
ϵ Tau.....	4 28	19 10	G9.5 III	3.53	32	>1.4
α Aur.....	5 16	45 59	G8 III	0.7	2	1.16
			G0 III	0.6	...	0.71

© American Astronomical Society • Provided by the NASA Astrophysics Data System

with a hollow-cathode lamp, but I did not use one for these observations. Double-fiber scramblers are inefficient, and the additional loss of efficiency was unnecessary because the primary method of calibration of these observations is the I_2 cell, which does not require the use of a double-fiber scrambler since the I_2 spectrum will undergo the same shifts resulting from seeing and guiding errors as the stellar spectrum.

During 3 days of the observing run, I observed the unimaged daytime sky spectrum. For these observations, the shutter of the Coudé Feed telescope primary was closed, giving the fiber aperture a view of a white surface exposed to daylight. These observations are used to further calibrate the instrumentation and confirm the validity of the data analysis procedures (see § 5).

A serious systematic problem existed for the first 4 nights of the observing run. The CCD dewar was mounted on the FOE optical table with a three-point support. The center of the three points was directly under the center of mass of the dewar, but far to one side of the center of mass of the dewar with attached electronic saddle bags. Thus, as the liquid nitrogen in the dewar evaporated, the center of mass of the dewar-electronics system shifted. Once the center of mass moved far enough, the dewar would tilt to one side, causing the CCD to translate and rotate relative to the focal plane. This problem was seen as a drift in the spectrum across the detector in the early morning hours, and the cause was discovered and corrected on the fourth night of the run. The end result is a large-scale motion of the spectrum across the CCD, which complicates the data analysis additionally (see § 4.4).

4. DATA REDUCTION AND ANALYSIS

4.1. *Calibration*

Echelle spectrographs typically suffer from instabilities caused by environmental changes around the spectrograph, or temporal variations in the illumination of the collimator due to changes in seeing and pointing errors of the telescope (see Griffin & Griffin 1973; Ramsey 1988). Very small motions of spectrograph optical elements can result in large apparent Doppler shifts; thus, it is necessary to observe the target star and wavelength calibrator simultaneously in order to calibrate out apparent Doppler shifts caused by spectrograph instabilities. One can either add a second channel to the spectrograph carrying the wavelength calibration information, or superimpose the wavelength calibration information onto the stellar spectrum. These techniques each have their advantages and disadvantages, but the choice between the two is almost entirely dependent on the intrinsic stability of the spectrograph used. An I_2 absorption cell is used as the primary wavelength calibrator for these observations because, as pointed out in § 3, the FOE is not an intrinsically stable spectrograph. Since a second channel already existed on the FOE there was no disadvantage in using a ThAr hollow-cathode emission lamp as a secondary calibrator.

4.2. *Determination of Spectral Shift*

The data processing is split into two distinct phases, reduction and analysis. Here I define data reduction as the steps required to produce calibrated one-dimensional spectra from CCD images, and the data analysis as the determination of the Doppler shift from the one-dimensional spectra and any further processing. The techniques for data reduction of CCD echelle spectrograph data are well known and will not be discussed here. The reduction and analysis was performed using routines written in IDL (Interactive Data Language).

The fundamental difference between planetary search observations and asteroseismology observations is the cadence of the observations. Planetary searches involve a few observations per year for each star in the survey. Asteroseismology observations involve hundreds of exposures per night and sometimes solar observations during the daytime for calibration purposes. In order to detect unusual systematic problems in time to correct them during the observing run, some data analysis needs to be performed during the run. Therefore, there is an emphasis in asteroseismology on data analysis algorithms that can be computed quickly. Computational resources available during an observing run are typically limited, especially when observations are acquired both day and night. The data analysis procedures used by Marcy & Butler (1992) focus on derermining the Doppler shift for individual spectral lines or small groups of lines. They determine the point-spread function (PSF) for a segment of a echelle order and deconvolve the spectral segment. This, however, is time consuming because it requires line identification, determination of the PSF, and deconvolution of the spectrum. With the need for computational speed in mind, asteroseismologists would like to determine the Doppler shift of each echelle order of the spectrum, rather than determining the shift for each line or small sections of the order individually. This decreases the number of computations required to calculate the shifts.

One can describe the spectra when using the I_2 absorption cell by

$$D = S(\lambda + \delta_S)I(\lambda + \delta_I)\,, \tag{1}$$

where D represents the data (a stellar spectrum with I_2 spectrum superimposed), S represents the stellar spectrum, I represents the I_2 spectrum, and δ_S and δ_I represent the shifts of the stellar and I_2 spectra respectively. In equation (1), I am ignoring the PSF of the spectrograph and other complications. All the stellar lines between 500 and 630 nm are blended with I_2 lines because the I_2 spectrum is saturated with absorption lines in this spectral range. Any data analysis algorithm must take this blending into account in order to determine Doppler shifts to high precision.

Figure 1*a* shows the spectrum of α Aur for one echelle order. Figure 1*b* is the I_2 spectrum taken using a quartz lamp source for the same echelle order. Note the molecular band structures and the fact that the I_2 lines are not resolved. Figure 1*c* is the spectrum of α Aur with the I_2 spectrum superimposed.

To determine the spectral shifts of these observations, I used the least-squares technique, analyzing each echelle order separately. To demonstrate this technique, I will first demonstrate it for an unblended spectrum (i.e., star spectrum without I_2 superimposed). The details of the least-squares technique for blended spectra are in the Appendix.

For spectra without absorption spectra superimposed, one can describe the data to first order in δ_S using a Taylor expansion

$$D(\lambda + \delta_S) \approx S(\lambda) + \delta_S \left.\frac{\partial S}{\partial \lambda}\right|, \tag{2}$$

where D represents the data, S represents the stellar spectrum (stellar template), and δ_S represents the shift of the

© American Astronomical Society • Provided by the NASA Astrophysics Data System

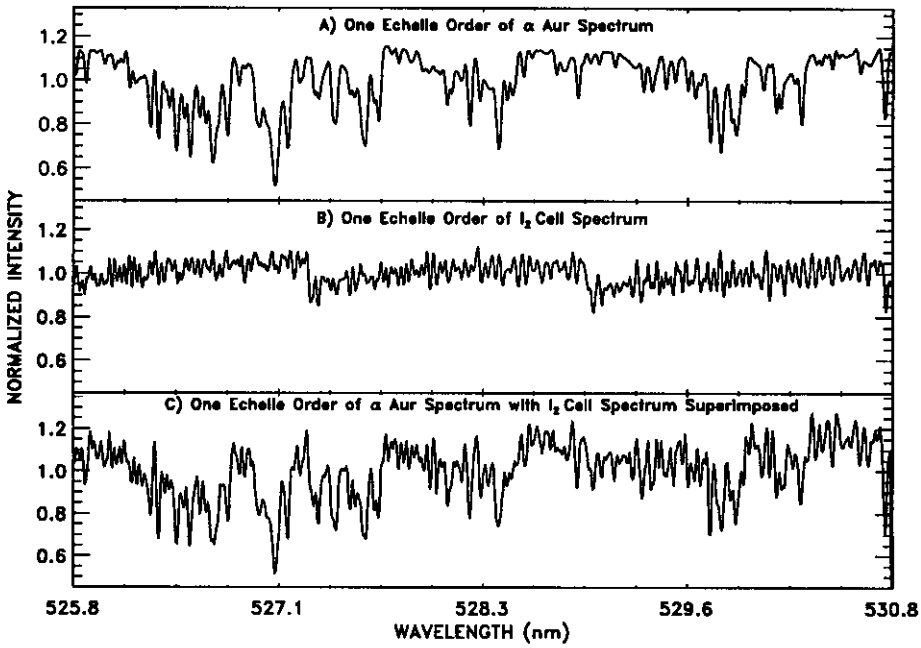

FIG. 1.—(*a*) One echelle order of α Aur spectrum. (*b*) The same echelle order of I_2 spectrum taken using a quartz lamp source. Note the molecular band structures and that the I_2 lines are not resolved. (*c*) The same echelle order of α Aur spectrum with the I_2 spectrum superimposed. I normalized the average intensities to 1.0 in this figure.

stellar spectrum. Using the method of least-squares, one defines the cost function (also known as the figure-of-merit function) as

$$\chi^2 = \sum_{i=1}^{N} \frac{1}{\sigma_i^2} \left(D_i - S_i - \delta_S \left. \frac{\partial S}{\partial \lambda} \right|_i \right)^2 , \quad (3)$$

where D_i represents the observation, S_i represents the stellar template, and i represents the pixel number. One determines the spectral shift by locating the minimum of the cost function by setting the partial derivative of χ^2 with respect to δ_S equal to zero,

$$0 = \frac{\partial \chi^2}{\partial \delta_S} = -2 \sum_{i=1}^{N} \frac{1}{\sigma_i^2} \left(D_i - S_i - \delta_S \left. \frac{\partial S}{\partial \lambda} \right|_i \right) \left(\left. \frac{\partial S}{\partial \lambda} \right|_i \right) . \quad (4)$$

Solving equation (4) for δ_S, one has

$$\delta_S = \sum_{i=1}^{N} \left[\frac{1}{\sigma_i^2} (D_i - S_i) \left(\left. \frac{\partial S}{\partial \lambda} \right|_{\lambda_i} \right) \right] \Big/ \sum_{i=1}^{N} \left[\frac{1}{\sigma_i^2} \left(\left. \frac{\partial S}{\partial \lambda} \right|_{\lambda_i} \right)^2 \right] , \quad (5)$$

where S represents the template spectrum, D represents the observed spectrum, and σ_i represents the standard deviation of the observations about the actual value D_i. The uncertainty of the estimation of δ_S is

$$\sigma_{\delta_S} = \left\{ \sum_{i=1}^{N} \left[\frac{1}{\sigma_i^2} \left(\left. \frac{\partial S}{\partial \lambda} \right|_{\lambda_i} \right)^2 \right] \right\}^{-1/2} . \quad (6)$$

If photon noise dominates the noise in the observation, $\sigma_i^2 \approx S_i$, equation (6) becomes the equation for the photon-limited Doppler precision (PLDP) (see Brown 1990; Connes 1985).

The blending of the spectra when the I_2 spectrum is superimposed complicates the least-squares technique. The equations for the shift in the stellar spectrum, δ_S, the shift in the absorption cell spectrum, δ_I, and the equations for the estimation of the errors of the shifts determined, are in the Appendix. I am using a linear least-squares even though the spectrum product, $S(\lambda + \delta_S)\, I(\lambda + \delta_I)$, is the result of a non-linear process; therefore, I must iterate to obtain an accurate solution. Using Fourier interpolation, I shifted the S and I templates by δ_S and δ_I, respectively, and iterated. The errors in the template spectrum are assumed to be small compared to the errors of the observation. This assumption will be valid if the template is constructed by combining a large number of observations.

4.3. *Templates*

The least-squares method requires the use of template spectra, $S(\lambda)$ and $I(\lambda)$. By combining a number of spectra taken of the target star without the I_2 cell in the beam, I generated an observed stellar template $S_{obs}(\lambda)$. By combining a number of spectra of a quartz lamp with the I_2 cell in the beam, I generated an observed I_2 template, $I_{obs}(\lambda)$. I also generated alternate observed I_2 templates by combining observations of rapidly rotating hot stars with the I_2 cell in the beam. These stars have few, broad-lines and are sometimes preferable to the quartz lamp for illuminating the I_2 cell, since the hot star will illuminate the I_2 cell in the same manner as the target star. The disadvantage is that these stars are not completely devoid of structure in their spectra. These template spectra were generated using images taken over the course of the run, so the relative shifts must be calculated before the spectra can be combined. The least-squares (see eq. [5]) approach was used to determine the shifts.

4.4. *CCD Instabilities and Imperfections*

Motion of the CCD relative to the spectrograph results in serious problems in determining high-precision radial velocities. CCD motion causes stretching in the spectrum and alters the PSF of the spectrograph (the PSF will be discussed in detail in § 5). This can be caused by motion of the KPNO dewar relative to the focal plane of the spectrograph camera or motion of the CCD within the dewar. Motions of the CCD within the dewar are the result of the thermal cycling of the liquid nitrogen dewar (see Smith 1990; Brown et al. 1991).

© American Astronomical Society • Provided by the NASA Astrophysics Data System

During the course of this observing run, the CCD rotated about an axis parallel to the cross-dispersion direction. This problem was especially acute during the early nights of the run when the CCD mount was loose, but it persists throughout the run. This rotation results in stretching of the observed spectra because the separation between CCD pixels in the focal plane changes with the angle of the CCD relative to the focal plane. Unfortunately, thinned CCDs of this era are not flat, so the spectral stretching is of higher order than first order. Therefore, I determine the shift for a segment of the echelle order defined by a sliding boxcar function and de-stretch the spectra using a low-order polynomial fit to the segment shifts.

5. RESULTS

On each night of the observing run, I obtained several exposures of each of the program stars without the I_2 cell in the beam for use as reference spectra. The primary purpose of these observations was to generate the stellar templates discussed in § 4.3; however, these observations were taken with the ThAr lamp illuminating the second fiber for use as a wavelength reference. I compared the shifts of the ThAr spectra to the shifts of the stellar spectra, uncomplicated by blending with the I_2 spectra. Figure 2 shows the shifts, in pixels, of the stellar spectra relative to the ThAr spectra, with the ephemeris velocity, and the binary motion in the case of α Aur, removed. I use a weighted mean to combine the shifts determined for each echelle order. It is immediately clear that there is a large systematic error present because the velocities of all four stars follow the same pattern.

There are a number of possible sources for the systematic error evident in Figure 2. The most likely source of the systematic errors when using the ThAr spectrum as the wavelength reference is the incomplete scrambling of the light by the single optical fiber, resulting in variations of the collimator illumination from night to night. At the beginning and end of each observing night, I removed the stellar fiber from its mount on the Coudé Feed in order to obtain flat-field and other calibration exposures. Therefore, the alignment of the optical fiber relative to the telescope beam varied from night to night. Changes in the alignment, along with the incomplete scrambling by the single fiber, may have resulted in variations in the collimator illumination that, coupled with aberrations in the ruling of the echelle grating, simulate Doppler shifts of the star spectra relative to the ThAr spectra. Another possible source of this systematic error could be changes in the relative line intensities of the ThAr lines resulting from changes in the alignment of the optical fiber relative to the cathode of the ThAr lamp, or aging of the lamp.

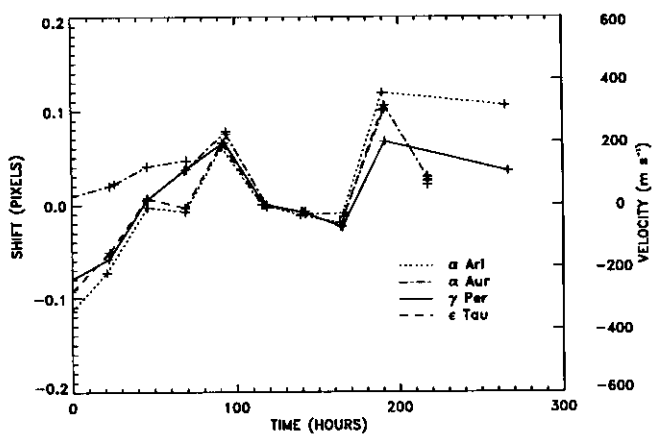

FIG. 2.—The shifts of the stellar spectra relative to the ThAr spectra with the ephemeris velocity and the binary motion, in the case of α Aur, removed. A weighted mean was used to combine the shifts determined for each echelle order. The result shows a systematic error giving all four stars the same velocity profile.

The systematic error might also be the result of changes in the relative position of the fibers at the slit. The separation between the stellar suborder and ThAr suborder (here I refer to spectra from different optical fibers, but of the same order of the echelle grating, as suborders) should be constant in a stable system. However, the data reduction indicates that the suborder separation varies by as much as 0.2 pixels and can vary on short timescales. Variation in the suborder separation can be the result of the CCD rotating about an axis that is parallel to the dispersion direction, or of relative motion of the slit fibers. During one set of flat-field exposures taken 1 hr after the dewar was filled with liquid nitrogen, the suborder separation changed by an amount equivalent to the CCD tilting by 4° over a half-hour time span. This is a large motion, especially considering the short timescale, whether it is the CCD or the slit that is moving. If the slit fibers are shifting their relative position by this amount in the cross-dispersion direction, they may also be moving in the dispersion direction, which would simulate a Doppler shift.

Smith (1990) used the KPNO TI3 CCD for high-precision radial velocity observations of γ Vir and reported that the shape of the CCD surface changed in a complicated manner owing to a combination of temporal and spatial gradients on the CCD resulting from the thermal cycling of the liquid nitrogen in the dewar. However, Brown et al. 1991) were able to obtain a short-term velocity precision of better than 3 m s^{-1} using the TI3 detector, the FOE, a ThAr lamp reference, and a double-fiber scrambler.

Another possible source of the systematic error could be changes in the spectrograph PSF resulting from instabilities in the spectrograph's optical elements. It is clear that the CCD position is not stable for these observations. Motion of the CCD results in changes in the PSF that are a function of time and position on the CCD. The PSF, $P(x)$, can also change as a result of variations in the focus and alignment of the spectrograph elements. These changes in the PSF can simulate Doppler shifts. If the PSF of the spectrograph varies as a function of time, error is introduced into the determination of the Doppler shift.

Since this systematic error persists in the velocities of the stellar spectrum relative to the ThAr reference for images taken with the I_2 cell in the beam, the remainder of the results presented here use the I_2 spectra as the wavelength calibration source.

Figure 3 shows the Doppler shifts of the α Aur spectra relative to the I_2 spectra on a night when observations were concentrated on Capella. The shift due to the observatory's motion relative to the Sun resulting from the Earth's rotation and revolution has been removed, as has the binary motion of the Capella system. The different symbols represent different orders of spectra (some symbols are used for more than one order). Late in the night, the noise in the observations increased dramatically because of increasing clouds. The photon-limited Doppler precision for a single order in these observations is $\approx$0.015 pixels or 54 m s^{-1}. In

© American Astronomical Society • Provided by the NASA Astrophysics Data System

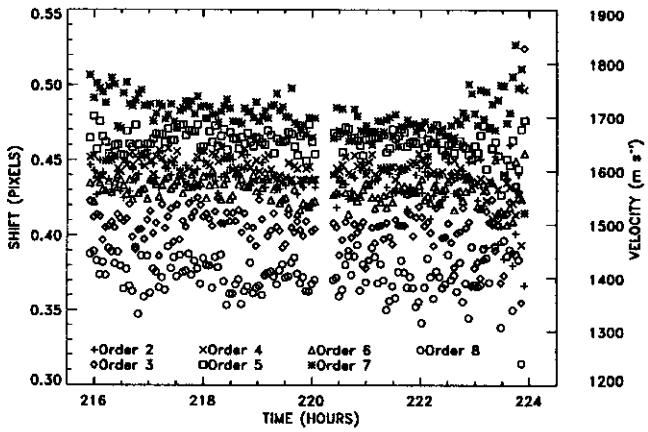

FIG. 3.—The relative Doppler shifts of the α Aur observations on a night when observations were concentrated on α Aur.

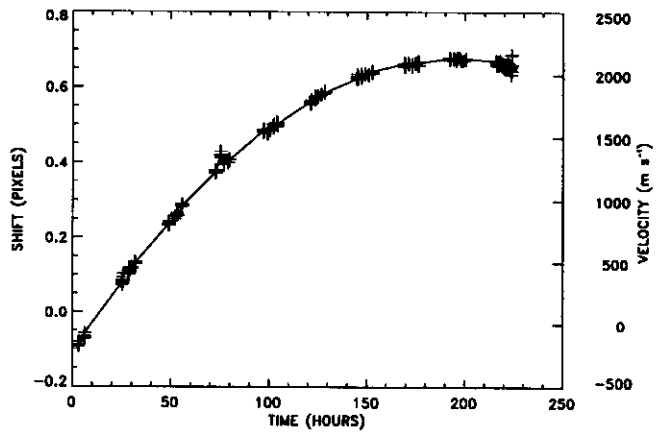

FIG. 5.—The relative Doppler shifts of the α Aur observations over the entire run. A weighted mean was used to combine the shifts determined for each echelle order. The motion of α Aur A about α Aur B is clearly visible.

Figure 3 it is evident that this precision has been attained within an order over a single night. But the variations from order to order are greater than the variation within the order.

These order-to-order variations may be the result of changes in the spectrograph PSF. The simulated Doppler shift due to changes in the PSF for the stellar and I_2 spectra may differ from one another, despite the fact that the spectra follow identical paths through the spectrograph and have identical changes in the PSF. The I_2 spectra have considerable fine structure; even with a Fourier transform spectrograph at $R = 500{,}000$ the lines of I_2 are unresolved. The stellar lines, however, are much broader and are easily resolved at the resolution of the FOE. Any high-frequency variations in the PSF will cause a simulated shift for the I_2 spectra but not for the stellar spectra, resulting in a relative shift. Figure 4*a* shows the ratio of the power spectra of a single echelle order of α Ari spectra with the I_2 spectra superimposed for two exposures taken 2 minutes apart. Figure 4*b* shows the ratio of the power spectra of a single echelle order of α Ari spectra with the I_2 spectra superimposed for two exposures taken 2 days apart. Variations in the PSF of the spectrograph will cause variations in the power spectra. It is clear from these ratios of power spectra that the spectrograph PSF is varying over timescales of days, but determining the quantitative effect of this variation on the Doppler velocities observed is beyond the scope of this paper.

If the order-to-order variation is assumed to be systematic noise and is removed by averaging the shifts for each of the orders together, the photon-limited Doppler precision for each exposure is ≈ 0.006 pixels or 21 m s^{-1}. I used a weighted mean to combine the shifts of each echelle order. I did not include orders 0 (480.2 nm–484.8 nm) and 1 (490.8 nm–495.5 nm) in the mean because they are beyond the spectral range of the I_2 lines. Also, I did not include order 9 (596.0 nm–602.5 nm) in the mean because the I_2 lines are weak near the end of the I_2 spectral range, and the CCD has a large number of cosmetic defects contaminating this order. Figure 5 shows the weighted average of the α Aur observations over the course of the entire run. The motion of α Aur A about α Aur B is clearly visible (period 104.0204 days, K 26.1 km s^{-1}; Hoffleit & Jaschek 1982).

I subtracted the ephemeris velocity, and the binary motion in the case of α Aur, from the weighted averages of the echelle orders. To remove any components with periods too long to be resolved with these data, I passed the time

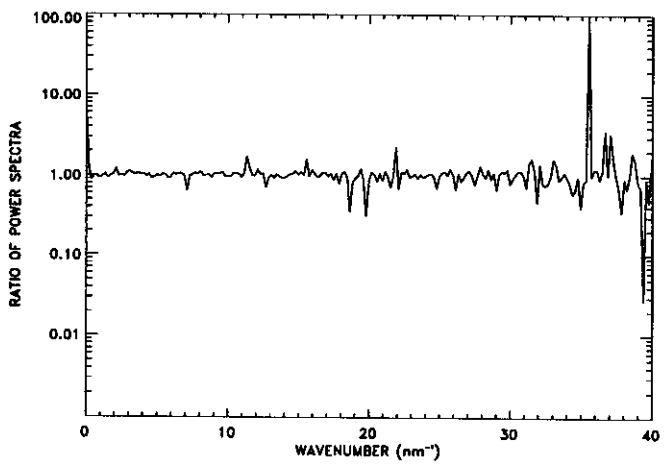

FIG. 4*a*

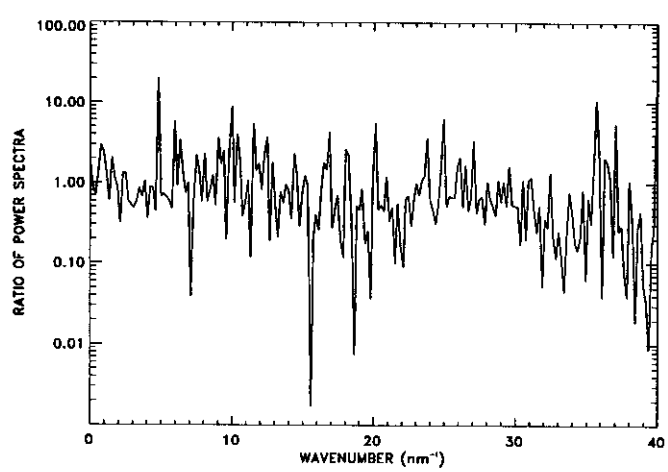

FIG. 4*b*

FIG. 4.—(*a*) The ratio of the power spectra of a single echelle order of α Ari spectra with the I_2 spectra superimposed for two exposures taken 2 minutes apart. (*b*) The ratio of the power spectra of a single echelle order of α Ari spectra with the I_2 spectra superimposed for two exposures taken 2 days apart. It is clear from these ratios of power spectra that the spectrograph point spread function is varying over timescales of days.

© American Astronomical Society • Provided by the NASA Astrophysics Data System

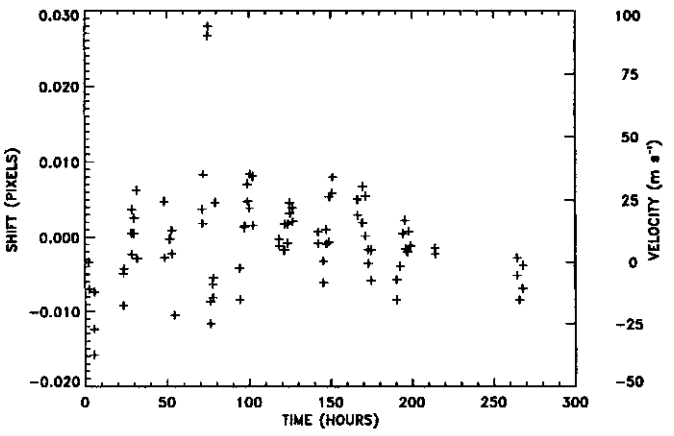

FIG. 6a

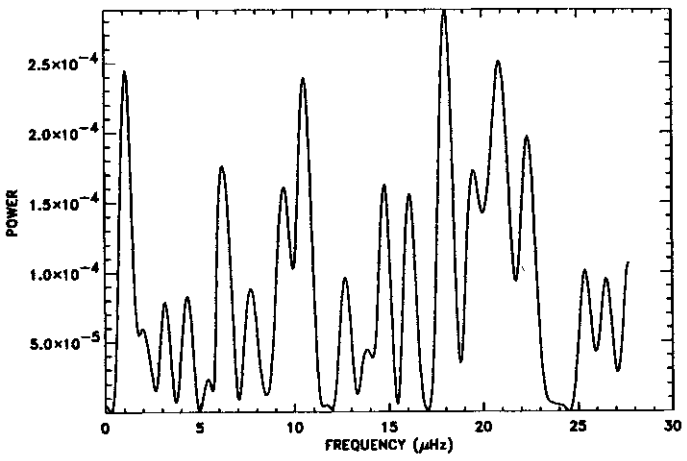

FIG. 6b

FIG. 6.—(*a*) The relative Doppler shifts of the α Ari observations over the entire run after smoothing with a high-pass filter. (*b*) The periodogram of the α Ari observations shown in (*a*).

series through a high-pass filter; first, I fitted a straight line to the data to remove any very long-period variations in the velocity such as motion due to a stellar companion (α Ari, α Aur, and γ Per are spectroscopic binaries). Then, I convolved the time series with a Gaussian of FWHM = 5 days and subtracted the result from the original time series in order to filter out radial velocity variations with periods too long to be adequately sampled by these data.

Figures 6–10 show the filtered average shifts of the stellar spectra relative to the I_2 spectra and periodograms for each of the four stars and for the solar observations. One can see from Figures 6*a*, 7*a*, 8*a*, 9*a*, and 10*a* that using the I_2 wavelength references does not suffer from the same systematic effect seen in the ThAr referenced data. The periodograms are computed using the Scargle (1982) algorithm for unevenly spaced data.

None of these four late-type giants have oscillations at the amplitude of Arcturus at any frequency sampled by these data. Figure 6*a* shows the averaged shifts of α Ari, and Figure 6*b* shows the periodogram of these data. Both figures show that there are no pulsations in the frequency range sampled above the noise level of 15 m s^{-1}.

Figure 7*a* shows the averaged shifts of α Aur A (spectroscopic primary of Capella), and Figure 7*b* shows the periodogram of these data. There is a possible 5 day period to these data with an amplitude of about 20 m s^{-1}, but a period of this length is poorly sampled by a observing run of only 10 days. There is also the added complication of the spectrum of α Aur B, which has not been taken into account in this analysis.

Figure 8*a* shows the averaged shifts of γ Per, and Figure 8*b* shows the periodogram of these data. Here there is a power peak at 6.2 μHz (1.9 days) with an amplitude equivalent to 16 m s^{-1}, but the power in this peak is almost entirely attributable to the outlier point at 77 hr. With this outlier removed from the data set, the peaks at 4.1 μHz (2.8 days) and its apparent harmonic at 15.8 μHz (0.7 days) dominate. Further analysis using PSF modeling would be required to reduce the noise level of these data to assign any useful significance to these peaks.

Figure 9*a* shows the averaged shifts of ε Tau, and Figure 9*b* shows the periodogram of these data. There are fewer observations of ε Tau because the exposure times were longer. The signal-to-noise ratio for these data is also lower than for the other stars. Both figures show that there are no pulsations in the frequency range sampled above the noise level of 20 m s^{-1}.

The solar observations where taken over a 60 hr period during the run for use as an additional calibrator. These

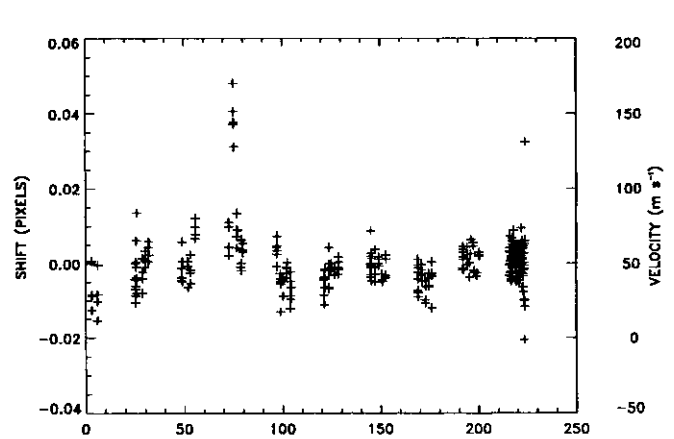

FIG. 7a

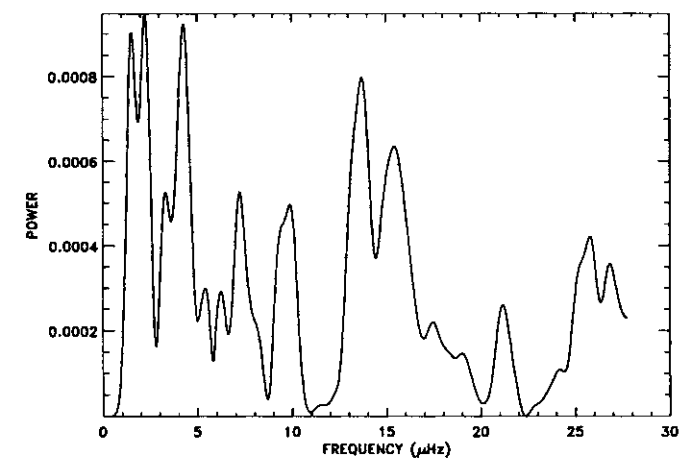

FIG. 7b

FIG. 7.—(*a*) The relative Doppler shifts of the α Aur observations over the entire run, with the binary motion removed, and smoothed using a high-pass filter. (*b*) The periodogram of the α Aur observations shown in (*a*).

© American Astronomical Society • Provided by the NASA Astrophysics Data System

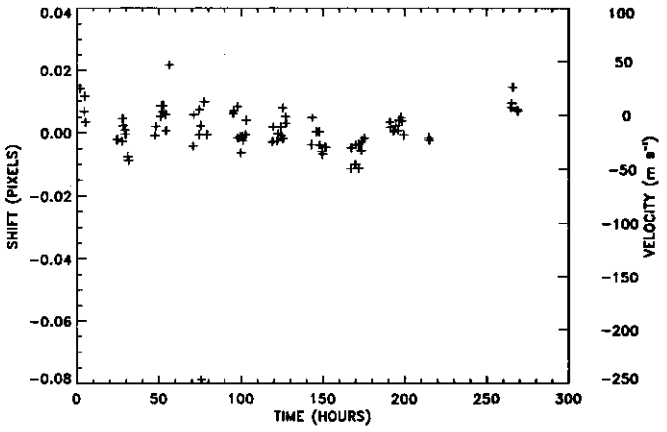

FIG. 8*a*

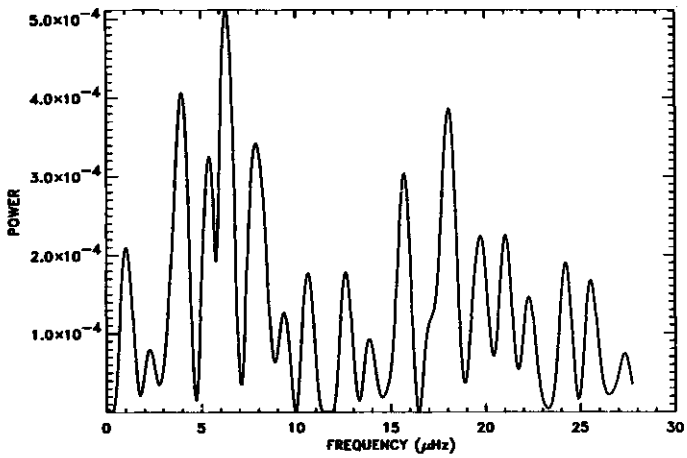

FIG. 8*b*

FIG. 8.—(*a*) The relative Doppler shifts of the γ Per observations over the entire run after smoothing with a high-pass filter. (*b*) The periodogram of the γ Per observations shown in (*a*).

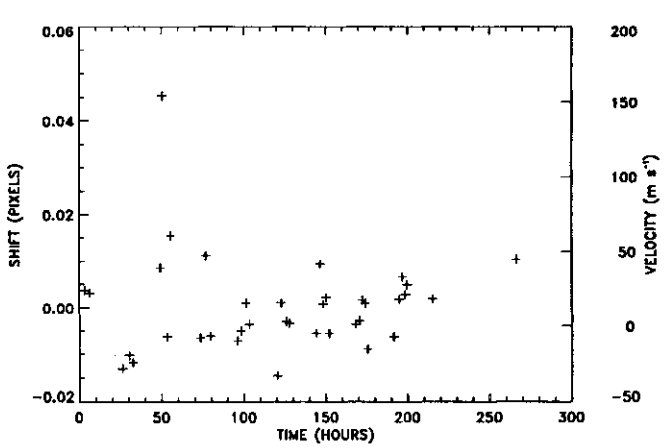

FIG. 9*a*

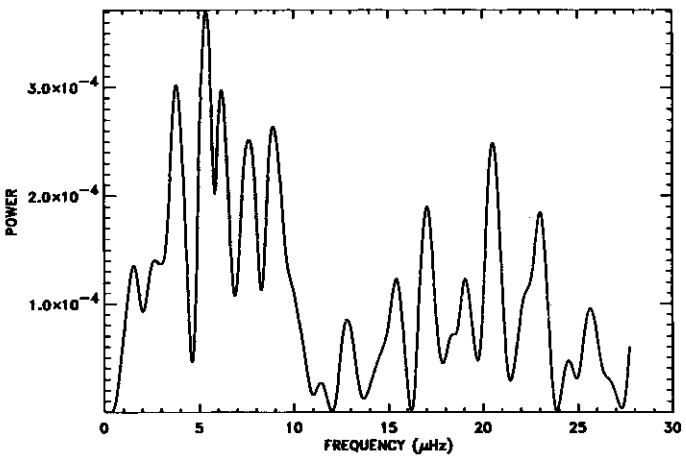

FIG. 9*b*

FIG. 9.—(*a*) The relative Doppler shifts of the ϵ Tau observations over the entire run after smoothing with a high-pass filter. (*b*) The periodogram of the ϵ Tau observations shown in (*a*).

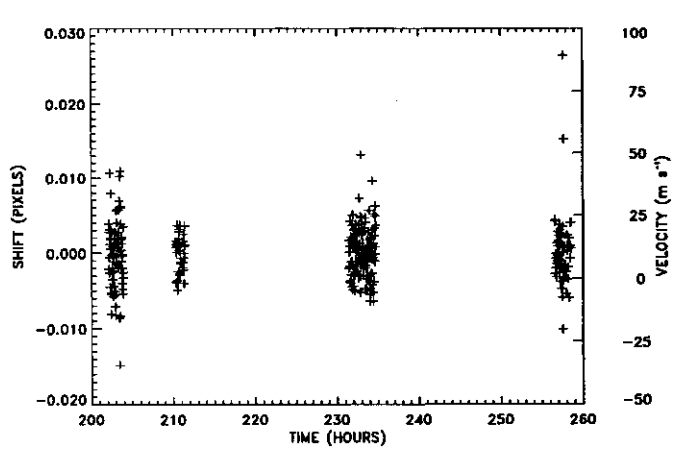

FIG. 10*a*

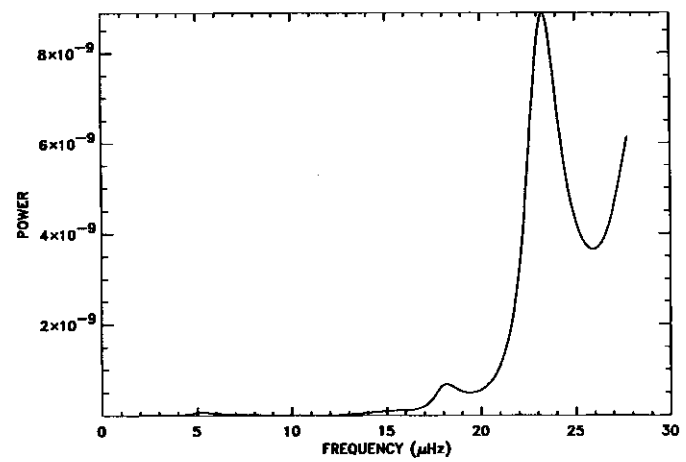

FIG. 10*b*

FIG. 10.—(*a*) The relative Doppler shifts of the solar observations over all day observations were made during the run after smoothing with a high-pass filter. (*b*) The periodogram of the solar observations shown in (*a*).

© American Astronomical Society • Provided by the NASA Astrophysics Data System

data were intended to confirm the stellar origin pulsations if all the stars demonstrated pulsations. The signal-to-noise level for these data is higher than for the stellar data. As expected, there are no pulsations at these periods in the solar data. Figure 10*a* shows the averaged shifts of the solar spectrum, and Figure 10*b* shows the periodogram of these data.

6. CONCLUSIONS

Oscillations of the amplitude and period observed on Arcturus were not observed on any of the four late-type giants observed in this campaign. This raises a number of questions: Is there some property of Arcturus, such as its composition or age, that separates it from these other late-type giants? Are the oscillations with this period and amplitude unstable and only an occasional phenomenon? The papers of Smith et al. (1987), Cochran (1988), and Belmonte et al. (1990) are conclusive in their detection of oscillations on Arcturus, but they are not at all conclusive that the amplitude and period of these oscillations are stable. The observations of Smith et al. and Cochran overlap for three days in 1988 and concur that there is a night-to-night variation in radial velocity of order 150 m s^{-1}. Nevertheless, the observations of Smith (1982) should have detected oscillations of the amplitude and period observed by the others but did not. Hatzes & Cochran (1994) report that observations made in 1992 June show oscillations with periods of 2.46 days and 3.8 days, but they do not see the 1.84 day period observed in 1990, and they suggest that Arcturus has switched pulsation modes (They also report 500 m s^{-1} oscillations with a 233 day period [Hatzes & Cochran 1993]). Therefore, it is likely that the pulsation modes of stars like Arcturus have short lifetimes, but the question remains whether the four stars observed in this campaign are structurally different from Arcturus, or just in a quiescent state, as Arcturus may have been when Smith (1982) observed it in 1980. Clearly, a larger sample of late-type giants, including Arcturus, need to be observed over long timescales in order to resolve these questions.

By observing several giants with a range of effective temperature, one should gain some understanding of the stellar conditions required to support Arcturus-like pulsations. In particular, knowing the variation of pulsation amplitude with effective temperature would help determine whether pulsations in giants are driven by acoustic noise from the convection zone (as in the Sun), or by other mechanisms. Furthermore, the period of a star's *p*-mode pulsation in the fundamental scales inversely as the square root of the star's mean density. Thus, if pulsations are detected, constraints can be placed on the stellar radii and masses. Finally, the photospheric acoustic waves in giants may be connected to chromospheric phenomena and mass loss in these stars. One question of interest is whether there is a correlation between whether a late-type giant oscillates and the coronal and wind dividing lines (Haisch, Schmitt, & Rosso 1991). Knowledge of the Doppler spectra would allow us to begin to understand these connections.

While I have made progress in developing the techniques for very precise radial velocity measurements, further gains are required to reach the precision required for the goal of observing oscillations on Sun-like stars. It is clear that one gains considerable advantage using a spectrograph stabilized for high-precision radial velocity observations. Hollow-cathode lamps as wavelength references are especially susceptible to systematic errors resulting from instabilities of the spectrograph. The level of these systematic errors will depend on the spectrograph and the environmental conditions. For an unstabilized system, the absorption cell reference is superior to the hollow-cathode lamp reference because the reference follows an optical path identical to the stellar spectrum. But changes in the spectrograph PSF will still result in sinmulated Doppler shifts of the stellar spectrum relative to the absorption cell reference.

With a stabilized spectrograph, a hollow-cathode lamp could be used as a short-term wavelength reference, with periodic calibration with the I_2 cell to establish a long-term wavelength reference. The Advanced Fiber Optic Echelle (AFOE) is an instrument designed to operate in this manner to detect stellar oscillations and search for planets orbiting stars other than the Sun (see Noyes et al. 1993a, b; Brown et al. 1994). In the future, more observations of late-type giants, including Arcturus, are planned using the AFOE. Since the AFOE is a stabilized system, the spectral shifts will always be small—dominated by Earth's rotation and revolution, instead of systematic effects—so the data analysis procedures can be simplified accordingly.

I thank Timothy M. Brown and Robert Rosner for their scientific support for this project and others I have undertaken over the course of my graduate career. I express my gratitude to the High Altitude Observatory for its financial support through a Gordon Newkirk Graduate Research Assistantship. I also thank the High Altitude Observatory and the University of Chicago for financial support and NASA (at the University of Chicago) for partial support of my research. I also appreciate the telescope and instrument time granted to me by KPNO and the TAC. I have benefited from many conversations on iodine absorption cell and data analysis with Geoff Marcy and R. Paul Butler. I also thank Linda Croom, Louise Beierle, Greg Card, and the HAO staff for their assistance, Jesper Schou for late-night commiseration, Brenda Willett for repeated reinforcement, and Jill and Jim Lauroesch for help editing this manuscript.

I utilized SIMBAD III and ADS in the preparation of this manuscript.

APPENDIX

DETERMINING THE STELLAR SPECTRAL SHIFT RELATIVE TO THE IODINE SPECTRUM USING THE LEAST-SQUARES TECHNIQUE

The stellar spectrum with iodine spectrum superimposed can be described by

$$D(\lambda, \delta_S, \delta_I) = S(\lambda + \delta_S)I(\lambda + \delta_I) \quad \text{(A1)}$$

© American Astronomical Society • Provided by the NASA Astrophysics Data System

(see eq. [1]), where $D(\lambda, \delta_S, \delta_I)$ represents the data (a stellar spectrum with I_2 spectrum superimposed), S represents the stellar spectrum, I represents the I_2 spectrum, and δ_S and δ_I represent the shifts of the stellar and I_2 spectra, respectively. Expanding the functions on the right-hand side of equation (A1) using a Taylor series and dropping terms above first order, one has, for small shifts δ_S and δ_I,

$$S(\lambda + \delta_S) \approx S(\lambda) + \delta_S \left.\frac{\partial S}{\partial \lambda}\right|_\lambda ,$$

$$I(\lambda + \delta_I) \approx I(\lambda) + \delta_I \left.\frac{\partial I}{\partial \lambda}\right|_\lambda . \tag{A2}$$

Combining equations (A1) and (A2) and dropping terms above first order, one has

$$D(\lambda, \delta_S, \delta_I) \approx \left[S(\lambda) + \delta_S \left.\frac{\partial S}{\partial \lambda}\right|_\lambda \right]\left[I(\lambda) + \delta_I \left.\frac{\partial I}{\partial \lambda}\right|_\lambda \right]$$

$$\approx S(\lambda)I(\lambda) + S(\lambda)\delta_I \left.\frac{\partial I}{\partial \lambda}\right|_\lambda + I(\lambda)\delta_S \left.\frac{\partial S}{\partial \lambda}\right|_\lambda . \tag{A3}$$

The cost function (also known as figure-of-merit function) is the sum of the squares over all spectral resolution elements of the observed spectrum (stellar and iodine spectra superimposed) minus the model spectrum (eq. [A3]) composed of the shifted stellar template multiplied by the shifted iodine template,

$$\chi^2 = \sum_{i=1}^{N} \frac{1}{\sigma_i^2} \left(D_i - S_i I_i - S_i \delta_I \left.\frac{\partial I}{\partial \lambda}\right|_i - I_i \delta_S \left.\frac{\partial S}{\partial \lambda}\right|_i \right)^2 , \tag{A4}$$

where D_i represents the observation (stellar spectrum with reference spectrum superimposed), S_i represents the stellar template, I_i represents the superimposed reference template, σ_i represents the error in the observation, and i represents the pixel number. One then determines the spectral shifts by locating the minimum of the cost function (eq. [A4]) by setting the partial derivatives of χ^2 with respect to the parameters δ_S and δ_I to zero. The shift of the stellar spectrum, δ_S, and the shift of a superimposed reference spectrum, δ_I, are thus given by

$$\delta_S = \frac{cd - ae}{be - c^2} , \quad \text{and}$$

$$\delta_I = \frac{ac - bd}{be - c^2} , \tag{A5}$$

where

$$a = \sum_{i=1}^{N} \left[\frac{1}{\sigma_i^2} (S_i I_i - D_i) \left(I_i \left.\frac{\partial S}{\partial \lambda}\right|_i \right) \right], \qquad b = \sum_{i=1}^{N} \left[\frac{1}{\sigma_i^2} \left(I_i \left.\frac{\partial S}{\partial \lambda}\right|_i \right)^2 \right],$$

$$c = \sum_{i=1}^{N} \left[\frac{1}{\sigma_i^2} S_i I_i \left.\frac{\partial I}{\partial \lambda}\right|_i \left.\frac{\partial S}{\partial \lambda}\right|_i \right], \qquad d = \sum_{i=1}^{N} \left[\frac{1}{\sigma_i^2} (S_i I_i - D_i) \left(S_i \left.\frac{\partial I}{\partial \lambda}\right|_i \right) \right],$$

$$e = \sum_{i=1}^{N} \left[\frac{1}{\sigma_i^2} \left(S_i \left.\frac{\partial I}{\partial \lambda}\right|_i \right)^2 \right]. \tag{A6}$$

The estimated errors in the determination of δ_S and δ_I are given by

$$\sigma_{\delta_S} = \left(\frac{e}{be - c^2} \right)^{1/2}, \qquad \sigma_{\delta_I} = \left(\frac{b}{be - c^2} \right)^{1/2} . \tag{A7}$$

So the error in determining the shift of the star relative to the reference, $\Delta\delta$, is given by

$$\sigma_{\Delta\delta} = \left(\frac{b + e}{be - c^2} \right)^{1/2} . \tag{A8}$$

REFERENCES

Bagnuolo, W. G., Jr., & Sowell, J. R. 1988, AJ, 96, 1056
Batten, A. H., Hill, G., & Lu, W. 1991, PASP, 103, 623
Belmonte, J. A., Jones, A. R., Pallé, P. L., & Cortés, T. R. 1990, ApJ, 358, 595
Brown, T. M., 1990, in ASP Conf. Ser., Vol. 8, CCDs in Astronomy, ed. G. H. Jacoby (San Francisco: ASP), 335
Brown, T. M., & Gilliland, R. L. 1994, ARA&A, 32, 37
Brown, T. M., Gilliland, R. L., Noyes, R. W., & Ramsey, L. W. 1991, ApJ, 368, 599
Brown, T. M., Noyes, R. W., Nisenson, P., Korzennik, S. G., & Horner, S. 1994, PASP, 106, 1285
Christensen-Dalsgaard, J., & Frandsen, S. 1983, Sol. Phys., 82, 469
Cochran, W. D. 1988, ApJ, 334, 349
Cochran, W. D., & Hatzes, A. P. 1990, Proc. SPIE, 1318, 148
Connes, P. 1985, Ap&SS, 110, 211
Fekel, F. C., Moffett, T. J., & Henry, G. W. 1986, ApJS, 60, 551
Gilliland, R. L., & Brown, T. M. 1988, PASP, 100, 754
Gilliland, R. L., et al. 1991, AJ, 101, 541
Gilliland, R. L., et al. 1993, AJ, 106, 2441
Griffin, R., & Griffin, R. 1973, MNRAS, 162, 243
Haisch, B., Schmitt, J. H. M. M., & Rosso, C. 1991, ApJ, 383, L15
Hatzes, A. P., & Cochran, W. D. 1993, ApJ, 413, 339

© American Astronomical Society • Provided by the NASA Astrophysics Data System

Hatzes, A. P., & Cochran, W. D. 1994, ApJ, 422, 366
Hoffleit, D., & Jaschek, C. 1982, The Bright Star Catalogue (4th rev. ed.; New Haven: Yale Univ. Obs.)
Kjeldsen, H., & Frandsen, S. 1992, PASP, 104, 413
Marcy, G. W., & Butler, R. P. 1992, PASP, 104, 270
Mihalas, D., & Binney, J. 1981, Galactic Astronomy (2d ed.; San Francisco: Freeman)
Noyes, R. W., Brown, T. M., Horner, S., Korzennik, S., & Nisenson, P. 1993a, in IAU Colloq. 137, Inside the Stars, ed. W. Weiss & A. Baglin (San Francisco: ASP), 752
———. 1993b, in ASP Conf. Ser., Vol. 42, GONG 1992: Seismic Investigation of the Sun and Stars, ed. T. M. Brown (San Francisco: ASP), 485
Pilachowski, C. A., & Sowell, J. R. 1992, AJ, 103, 1668
Pottasch, E. M., Butcher, H. R., & van Hoesel, F. H. J. 1992, A&A, 264, 138
Ramsey, L., Brown, T., Gilliland, R., & Noyes, R. 1991, in ASP Conf. Ser., Vol. 20, Frontiers of Stellar Evolution, McDonald Observatory 50th Anniversary, ed. D. L. Lambert (San Francisco: ASP), 614
Ramsey, L. W. 1988, in ASP Conf. Ser., Vol. 3, Fiber Optics in Astronomy, ed. S. C. Barden (San Francisco: ASP), 26
Ramsey, L. W., & Huenemoerder, D. P. 1986, Proc. SPIE, 627, 282
Scargle, J. D. 1982, ApJ, 263, 835
Smith, M. A. 1982, ApJ, 253, 727
———. 1990, AJ, 100, 1943
Smith, P. H., McMillan, R. S., & Merline, W. J. 1987, ApJ, 317, L79
Walker, G. A. H., Yang, S., Campbell, B., & Irwin, A. W. 1989, ApJ, 343, L21

© American Astronomical Society • Provided by the NASA Astrophysics Data System